



Investigation of CFRP cutting mechanism variation and the induced effects on cutting response and damage distribution

Qingxun Meng¹ · Jin Cai¹ · Hui Cheng² · Kaifu Zhang²

Received: 2 July 2019 / Accepted: 5 November 2019 / Published online: 2 January 2020
© Springer-Verlag London Ltd., part of Springer Nature 2020

Abstract

Machining of carbon fiber-reinforced polymers (CFRP) still remains a difficult procedure in the whole manufacturing process. One of the reasons is the cutting mechanism varies during machining, causing the inconsistency of surface integrity. This study intends to investigate the continuous variation of cutting mechanism and the induced cutting responses and damages. A novel experiment, with square and circular workpieces involved in cutting, was designed. A three-dimension micro-scale cutting simulation model was built. The experiment and simulation were combined to analyze the evolution and the correlation of cutting forces, machined surface roughness, sub-surface damage and the burr formation. The effects of rake angle and tool edge radius on chip formation and sub-surface damage were also presented. The conclusions are helpful to understand the damages generation during machining of CFRP.

Keywords CFRP · Cutting mechanism · Experiment · FEM simulation · Damages

1 Introduction

Carbon fiber-reinforced polymers (CFRPs) have gained a wide practical application, especially in the products that are sensitive to dead weight. In order to achieve long life cycle and high durability, it requires machining of near-net-shape CFRP parts with extraordinary precision and least defects to meet assembly needs. Being the typical machining methods (drilling, milling, turning, or trimming), materials are removed by cutting the edge according to specific cutting motion. Since fibers of different CFRP layers are in multiple orientations, the spatial relation between fibers and cutting edge varies continuously in cutting motion. Thus, how the fibers and matrix will be cut and separated to form chips, i.e., the cutting mechanism, varies through the whole machining process. The variation is considered contributing to fluctuation, vibration, and damages during machining. The authors believe almost all

unstable factors can be seen associating with the varying cutting mechanism. The most obvious evidences are cutting forces and damages distributed unevenly according to fiber orientation. In order to learn the dynamic behavior and create quasi-static status when machining CFRP, it is crucial to understand the variation of cutting mechanism and its effects on the distribution of cutting responses and damages.

Considering the CFRP layups and spatial relation of cutting edge and fibers, orthogonal cutting of unidirectional CFRP (UD-CFRP) has been taken as the most basic and representative unit [1]. In the past years, phenomena, data, and conclusions on CFRP cutting are obtained in literature by running simulations, conducting experiments, and building theoretical models. Calzada et al. [2] presented a finite element cutting model in a micro level. Fiber failure modes of four typical fiber orientation angles (FOA), namely, 0°, 45°, 90° and 135°, were reported. It was found when fiber orientations are 45° and 90°, the failure mode is crushing-dominated. When fiber orientations are 0° and 135°, the failure mode is bending-dominated. It was also found that the cutting force in simulation agreed well with that in experiment. The thrust force, however, is underestimated since the element delete technique was used. Gao et al. [3] establish a 3D micro-cutting model based on Ref. [2]. In the simulation, different chip morphologies and failure modes were presented with respect to the typical fiber orientations. The results showed

✉ Jin Cai
saucai@sau.edu.cn

¹ School of Aerospace Engineering, Shenyang Aerospace University, 37 South Daoyi Street, Shenyang 110136, Liaoning, China

² School of Mechanical Engineering, Northwestern Polytechnical University, 127 West Youyi Road, Xi'an 710072, Shaanxi, China

that the machined surface is smooth when fiber orientation is 45° and it becomes rougher at 135° . The cutting force increases with the cutting speed and cutting depth. The maximum and minimum values arrive at 90° and 45° respectively. Cheng et al. [1] reported a micro-scale cutting model with thermo-mechanical coupling. The simulation was divided into four groups according to fiber orientation. The deformation, stress distribution in cutting area, and cutting forces of 0° , 90° , 120° , 135° , and 150° fiber orientation was discussed. It was found that the fibers experience an extrusion shearing fracture rather than bending fracture when fiber orientation is acute. When fiber orientation turns to be obtuse, a large amount of bending occurs in fibers and the surface roughness goes much higher than that in acute fiber orientation. The cutting force was found larger than the thrust force regardless of fiber orientation. The cutting force becomes largest and the thrust force becomes smallest when fiber orientation is 90° . Yan et al. [4] studied fiber damage modes, energy distribution, cutting forces, and surface quality by using a micro-scale cutting simulation model. Liu et al. [5] built a micro-cutting FEM simulation model with random distribution of fibers in matrix. The influences of the cutting speed, cutting depth, and fiber orientation on the cutting process especially on the cutting force and machined surface were reported. It was found that the increase of the cutting speed is helpful to improve the quality of the machined surface. The cutting force value tends to increase when cutting depth increases. The machined surface quality is worse when fiber orientation is at 135° . Abena et al. [6] established a 3D numerical UD-CFRP orthogonal cutting model using the SPH method. The purpose is trying to reduce the effects of element deletion on thrust force prediction. In all the simulation models, the cutting mechanism is well described, the varying trend and the relation between cutting mechanism and cutting responses, however, still remain a lack of discussion.

Madhavan et al. [7] designed an experiment to obtain force and temperature data as a function of feed, speed, and fiber orientation. A UD-CFRP disk was involved in orthogonal cutting to study the influence of fiber orientation angle and cutting condition on forces and chip formation. The cutting force was found to depend on feed. It increases with FOA until an angle of 90° for a large feed, while it decreases beyond 65° for a low feed. Wang et al. [8, 9] did experiments to investigate edge trimming of unidirectional and multi-directional graphite/epoxy composite. Chip formation, cutting force, and surface topography were presented for various FOAs. Zitoune et al. [10] described chip formation, machined surface, and thermal behavior of long fiber composite by conducting orthogonal cutting experiments for the typical FOAs. More FOAs were involved in Wang's [11] experiment to investigate the effects of the FOA on cutting forces, surface roughness, and sub-surface damage during cutting of fiber-reinforced polymers (FRP). Henerichs et al. [12] investigated

the cutting forces, tool wear, workpiece damages, and delamination for different FOAs and tool geometry. Wang et al. [13] run experiments to study the evolution laws of fiber-matrix interface cracks when machining CFRP. The cracks were found to be determined mainly by fiber orientation. Su et al. [14] investigated the effects of cutting depth on chip formation mechanism based on experimental results. The characteristics of cutting force and chip formation for typical FOAs were reported. Voss et al. [15] conducted an experiment to study the effects of process parameter, tool geometry, and fiber orientation by milling of UD-CFRP. Extensive burrs were found when fiber orientation is 90° . Most of the experimental work in literature tends to present phenomena and trends, but little essential explanation about them were given by considering the continuous varying cutting mechanism. Some researchers [16–19] also tried to set up analytical models to study the CFRP cutting mechanism or forces. The models are capable of describing the continuous trends of cutting responses. The shortage of this method lies in a lot of assumptions that were involved during modeling.

In this study, the continuous varying cutting mechanism and its effects on cutting responses and damage distribution were investigated. A novel experiment, with square and circular workpieces involved in cutting, was designed to obtain cutting responses and the damages' data. The circular workpiece is used to measure the continuous variation values in the cutting process, while the square workpiece is tested in the same condition to reveal more details in cutting. The two types of workpieces are used to verify their results mutually. Also, a three-dimensional FEM model was built in micro-scale to simulate the chip formation process and the fibers out of plane displacement. The simulation model is able to predict how the fibers and matrix are cut step by step and then ejected to form a chip. By combining the experimental and simulation results, the cutting mechanism-related phenomena, such as cutting forces, machined surface roughness, sub-surface damage, burr, and the effects of tool geometry, are well explained.

2 Cutting test methodology

2.1 Experimental setup

The composite workpiece prepared for experiment was T300/7901. The stacking sequence was designed as $[0^\circ]_{20}$. The laminates were cured with the vacuum level of 0.6 to 0.1 Mpa. The temperature during curing experienced a step raising from room temperature to 125°C . Then, the laminated plates were cut into square and circular workpieces. The cutting tools used in the experiment were made of cemented carbide. The workpiece configuration, tool geometry, and cutting parameters used in the experiment is listed in Table 1.

Table 1 The parameters in experiment

	Parameter	Value
UD-CFRP	Square workpiece	60mm × 60mm × 4mm
	Circular workpiece	Φ60mm × 4mm
	Fiber diameter	8 μm
	Fiber volume	56.3%
Tool geometry	Rake angle	10°
	Relief angle	10°
Cutting parameters	Cutting depth	0.1 mm
	Cutting speed	5 m/min
	FOA of square workpieces	0°, 45°, 90° and 135°
	FOA of circular workpieces	Ranges from 0° to 180°

Figure 1 shows the experimental setup, where #1, #2, and #3 refer to workpieces, fixture, and dynamometer respectively. In the square-cutting test, the workpiece was fastened on the fixture, while the cutting tool was installed on the spindle. In the circular-cutting test, however, the workpiece was bounded to the spindle, while the cutting tool was fixed by the fixture. Their relative position was adjusted elaborately to keep the feed direction go exactly through the center of the circular workpiece. The fixture was screwed on a three-axis dynamometer (Kistler 9257A), which was connected to a Kistler 5073 charge amplifier. Then, the cutting force signals were transmitted to a HBM GEN2i type data acquisition. The sampling frequency was set to 2 kHz for each channel. All the cutting tests were conducted under dry condition. A microscopic camera was used to capture the chip formation process, which is helpful to observe how the fibers and matrix are cut and ejected.

2.2 Design of experiment

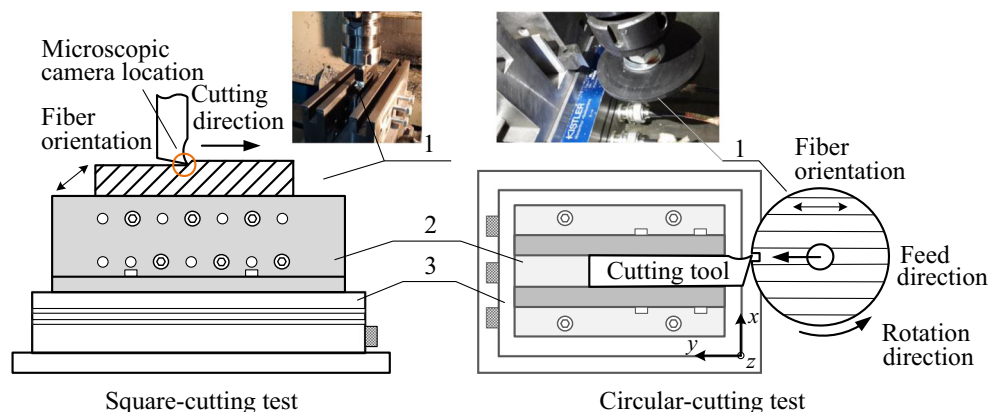
Both of the square- and circular-cutting tests were orthogonal cutting, and they were conducted under exact the same conditions with the same parameters, but without any interactions. The purpose of making such a combination lies in two aspects: (1) the measuring error will be reduced since the results of the two cutting tests can be used for mutual verification and (2)

more details refer to a specific FOA can be revealed in square-cutting test, while a general continuous trend of the cutting responses and damages with respect to all FOAs can be presented by circular-cutting test. On top of that, it is important to clarify that the square-cutting is able to duplicate the cutting mechanism on the corresponding segments of the circular workpiece. The cutting mechanism is dependent on fiber orientation, cutting tool geometry, and cutting parameters. Generally, when all the conditions are the same in square- and circular-cutting tests, the cutting mechanism is also considered the same. The most convincing proof is the configuration of the sub-surface damage since it is highly cutting mechanism dependent. The comparison of the sub-surface damage for the two tests is discussed in section 4.1. The sub-surface was examined as the following method. Small cuboids from both the circular and square workpiece were taken and polished. In order to protect the original sub-surface configuration during polishing, they were prepared using the cool mosaic method (as shown in Fig. 2).

3 Micro-scale orthogonal cutting simulation

The CFRP cutting simulation in literature was established in the so-called macro and micro ways. For the macro cutting

Fig. 1 The experimental set-up



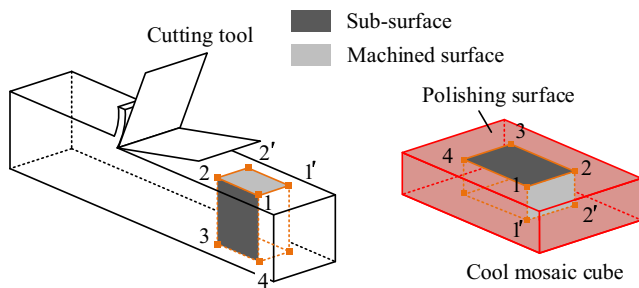


Fig. 2 Sub-surface damage measurement method

simulations [20–22], researchers considered the behavior of fiber and matrix together as equivalent homogenous materials, while in the micro cutting simulations [23–25], the properties of fiber and matrix were given separately and sometimes, an interface model was used to connect the fiber and matrix. Compared with macro models, the major advantage of micro models is it can reveal the chip formation process in detail. The simulation in this study is established based on the work in literature. It is used for further analysis and taken as supplements of experimental results.

3.1 Model definition

The model was built with reference to a small region of the square-cutting. It has good consistency with the real cutting because the real cutting can be seen as a geometric scale-up of the micro-scale cutting. Unlike square-cutting, however, the circular-cutting simulation is not able to achieve in the same way. This is because the extraordinary computing cost and the lacking of geometrical similarity in reality and micro-scale. As a compensation, more square-cutting simulations with various FOAs were involved to obtain the approximate continuous cutting responses. Besides the typical FOAs (0°, 45°, 90° and 135°), four more FOAs, namely 10°, 170°, 70° and 110°, are also introduced. The values are selected near

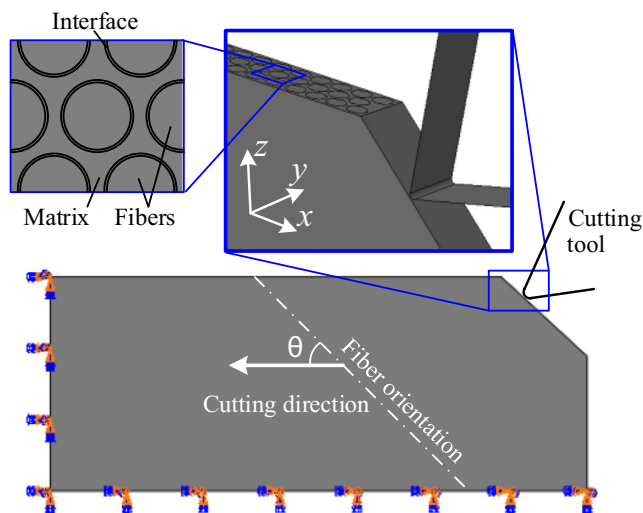


Fig. 3 Constitution of the simulation model in micro-scale

to the basic FOAs. Then the gradual variation of cutting mechanism can be tracked by combining the new selected and the basic FOAs responses. All the simulations were run using the commercial software ABAQUS (version 6.14). Figure 3 shows an example of the constitution of the micro model. It is assumed that the fibers distribute evenly in the epoxy matrix in the way shown in Fig. 3. The fibers’ volume and fiber diameter were made the same to that in experiment (shown in Table 1). The cutting direction was to the opposite of x -axis. The boundaries on the left and bottom were fixed. If the whole model is big enough compared with the cutting region, the effects of boundary could be neglected.

3.2 Fibers, matrix, and interface failure criteria

The fibers, epoxy matrix, and interface are characterized separately. Their properties are given in Table 2. The fibers are assumed as elastic anisotropy material. The anisotropic elasticity matrix is used to determine the elasticity behavior of fibers, but no plasticity is characterized. Eqs. (1) and (2) describe the tension and longitudinal compressive failure mode according to Hashin criteria [30, 31]. Considering the compressive effect in transverse direction, the fibers’ compressive failure in this direction is described in Eq. (3) according to maximum stress criteria.

Tension failure mode ($\sigma_{11} \geq 0$)

$$e_t = \left(\frac{\sigma_{11}}{X_t}\right)^2 + \left(\frac{\sigma_{12}}{S_{12}}\right)^2 + \left(\frac{\sigma_{13}}{S_{13}}\right)^2 = 1 \tag{1}$$

Longitudinal compression failure ($\sigma_{11} < 0$):

$$e_{c1} = \left(\frac{\sigma_{11}}{X_c}\right)^2 = 1 \tag{2}$$

Transverse compression failure ($\sigma_{22} < 0$ or $\sigma_{33} < 0$):

$$\begin{cases} e_{c2} = \left|\frac{\sigma_{22}}{Y_c}\right| = 1 \\ e_{c3} = \left|\frac{\sigma_{33}}{Y_c}\right| = 1 \end{cases} \tag{3}$$

where σ_{11} is the longitudinal stress; σ_{12} and σ_{13} are shearing stresses; σ_{22} and σ_{33} are transverse stresses; X_t and X_c are longitudinal direction tension and compression strength respectively; S_{12} and S_{13} are shearing strength; and Y_c is compression strength in transverse direction.

The epoxy matrix is characterized as elastic-plastic isotropic material. The constitutive law is shown in Fig. 4(a). The elastic behavior of epoxy matrix is described by Young’s modulus and Poisson ratio. After elastic deformation, the matrix is assumed to yield according to Mises criteria. Then, the stiffness degradation occurs as defined by Eq. (4):

Table 2 Material properties of fiber and epoxy matrix [26–29]

Materials	Properties	Values
Fiber	Elastic modulus	$E_{11} = 231 \text{ Gpa}, E_{22} = 15 \text{ Gpa}, E_{33} = 15 \text{ Gpa}$
	Poisson ratio	$\nu_f = 0.2$
	Tension strength	$X_t = 4.6 \text{ Gpa}$
	Compression strength	$X_c = 3.9 \text{ Gpa}, Y_c = 1.5 \text{ Gpa}$
	Shearing strength	$S_{12} = S_{13} = 1.5 \text{ Gpa}$
Matrix	Elastic modulus	$E_m = 3.35 \text{ Gpa}$
	Poisson ratio	$\nu_m = 0.35$
	Yield strength	$Y_m = 120 \text{ Mpa}$
Interface	Normal strength	167.5 Mpa
	Shear strength	25 Mpa
	Fracture energy	0.05 N/mm ²

$$E = (1 - D_m)E_m^0 \tag{4}$$

where D_m is the matrix damage variable; E_m^0 is the stiffness before degradation; E is the degraded stiffness. D_m varies from zero to unity as damage evolves. When the value equals to unity, the element stiffness decreases to zero and then, the material reaches final failure. D_m is calculated by Eq. (5):

$$D_m = \frac{\bar{u}^{pl}}{\bar{u}_f^{pl}} = \frac{L\varepsilon^{pl}}{\bar{u}_f^{pl}} \tag{5}$$

where \bar{u}^{pl} is equivalent plastic displacement; L is the characteristic element length; ε^{pl} is equivalent plastic strain; \bar{u}_f^{pl} is the equivalent plastic displacement at failure point and is given by Eq. (6):

$$\bar{u}_f^{pl} = \frac{2G^f}{Y_m} \tag{6}$$

where G^f is fracture energy and Y_m is yield strength.

Cohesive element is usually used to simulate interface behavior between different CFRP layers. In CFRP cutting, however, when using cohesive element as the interface of fiber and matrix,

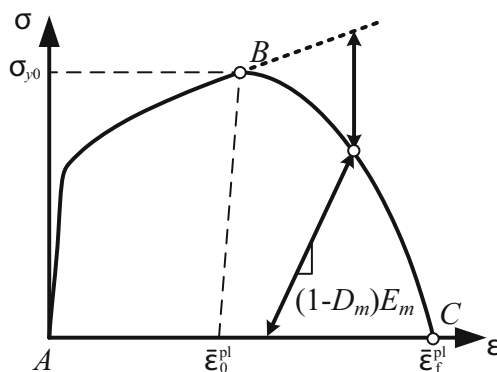


Fig. 4 Constitutive law of epoxy matrix

the simulation will abort due to excessive distortion. In this study, the interface is implemented by the elements with small thickness. The elements considered experience progressive damage during cutting. The damage initiation occurs when maximum normal or tangential stress reaches the strength. The progressive failure process was implemented with reference to [2, 3]. The properties of the interface are shown in Table 2.

4 Results and discussion

4.1 Simulation and experimental results

Figure 5 is the comparison of the results obtained from simulation, circular-, and square-cutting tests. As can be seen, for each FOA, the chip configuration in the simulation shows high accordance with that obtained from the square-cutting test. The sub-surface damage length in the circular- and square-cutting tests was in the same level. When FOA = 0°, the fibers on the top of the chip were lifted by the rake face and bended to failure, while the fibers near the cutting tip experienced buckling failure first then began to slide on the rake face. These can both be seen from the simulation result and the square-cutting test. The chip was continuous and curled. The fibers in the chip were found the longest in the four situations. There was almost no damage observed in the sub-surface according to the image of square and circular-cutting tests.

When FOA = 45°, according to the simulation, the fibers were cut into short fragments first and then were pushed upward along the rake face. It was found there was an obvious shearing in the chip ahead of the cutting tip. For this reason, there existed barely connections among the fibers and was causing the chip to be actually powder like. The same phenomenon was observed in the square-cutting test. The length of sub-surface damage in this situation was measured about 20 μm and 25 μm in the circular- and square-cutting tests respectively.

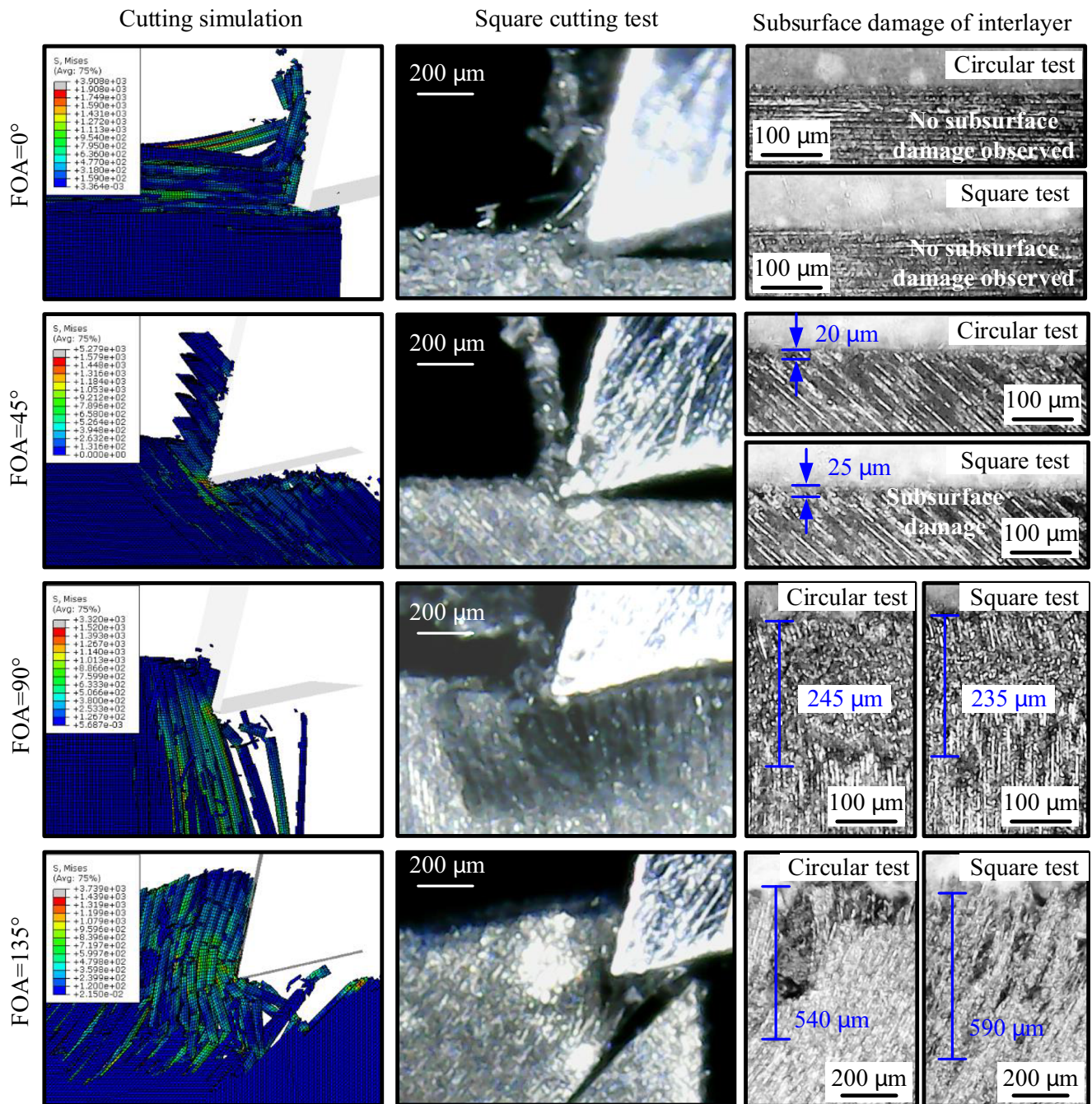


Fig. 5 Chip configuration and sub-surface damage of simulation and experiment

When FOA = 90°, the fibers were bended first and then being cut by the cutting edge. The shortest fibers in chips were measured in the four situations. Another phenomenon was found in both the simulation and the square-cutting test: the fibers in the very outside were pushed toward to the lateral direction, leaving a bunch of fibers not being cut by the cutting edge. This indicated that the deformation in cutting process can never be assumed as plane deformation. Further explanation will be presented in section 4.4. The length of sub-surface damage was found much larger

than that when FOA = 45°. The values recorded in circular- and square-cutting tests were 245 μm and 235 μm respectively.

When FOA = 135°, the fibers were not cut by the cutting edge but bended to failure by the rake face. The chip formation became extremely hard and severe damage was found in the cutting area. This can be seen from both the results of the simulation and the square-cutting test. The sub-surface damage was the severest in the four situations with the length reaching 540 μm in the circular-cutting test and 590 μm in the square-cutting test.

4.2 Variation of cutting mechanism

There are three stages in chip formation, namely failure initiation, cracks propagation, and chip removal. In the first stage, though the fibers or matrix is broken, they are still a part of the workpiece. In the second stage, the pressure from cutting tip transfers deeper causing more fibers to be cut and the cracks propagate further in the interface. The cutting chip does not form until the third stage where the freed fibers start to move along the rake face. Therefore, the description of cutting mechanism should be time-based. In this study, the cutting mechanism is summarized as three types: tearing type, crushing type, and bending type, which are illustrated in Figs. 6, 7, and 8 respectively. For each type, the cutting mechanism is described in the aforementioned three stages, and multiple FOAs are selected to reveal how the cutting mechanism type changes from one to another gradually.

The tearing type, which distinct feature is the Mode I fracture exists ahead of the cutting tip, can be observed when FOA is around 0°. Figure 6 shows the cutting mechanism of FOA =

0° and two adjacent FOAs (170° and 10°). The failure initiation of FOA = 0° occurs as the buckling stress in the fibers ahead of the cutting tip reaches the strength. Then, the fibers will be separated by the cutting wedge, causing cracks to propagate in the matrix along the cutting direction (Fig. 6b). Meanwhile, the fibers and matrix on top of the cutting tip are forced to slide on the rake face and then bended to form chips once the tension or compression stress (Fig. 6b and c) in the fibers exceeds the ultimate strength. As FOA increases gradually to 10°, the fibers tend to be pressed by the cutting tip, causing bending-induced stress in the fiber (Fig. 6d). Then, bending-induced stress may cause the failure of the interface in the sub-surface, which is the main source of sub-surface damage. When the cutting tip moves forward, the fibers and matrix are actually crushed to form a chip (Fig. 6e and f). As FOA changes to 170°, the rake face is playing a more significant role than the cutting tip. The failure initiation occurs more likely in the matrix and then extends to generate cracks (Fig. 6g and h). Similar to FOA = 0°, the fibers and matrix will slide on the rake face after failure initiation. The sliding trend,

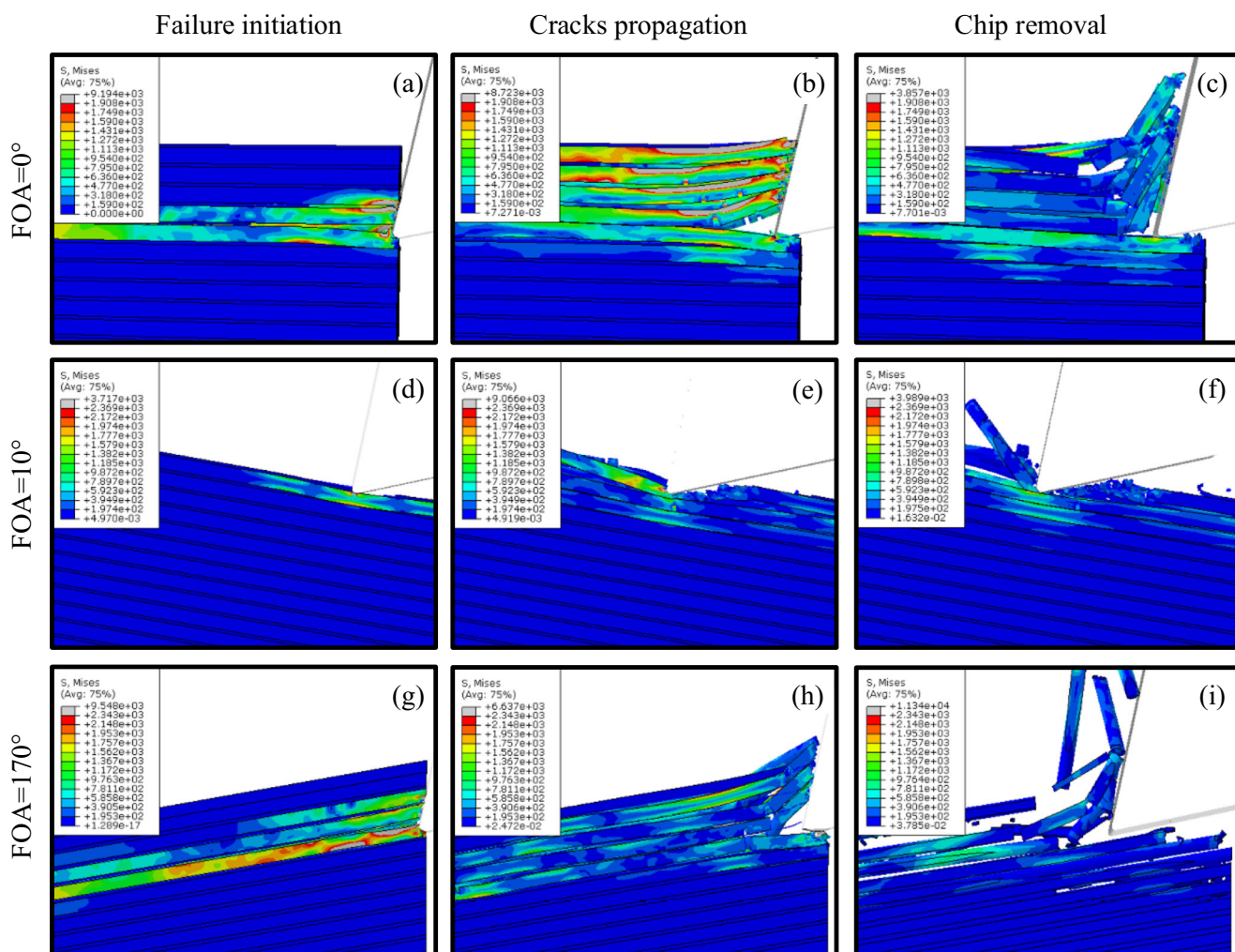


Fig. 6 Cutting mechanism variation of tearing type

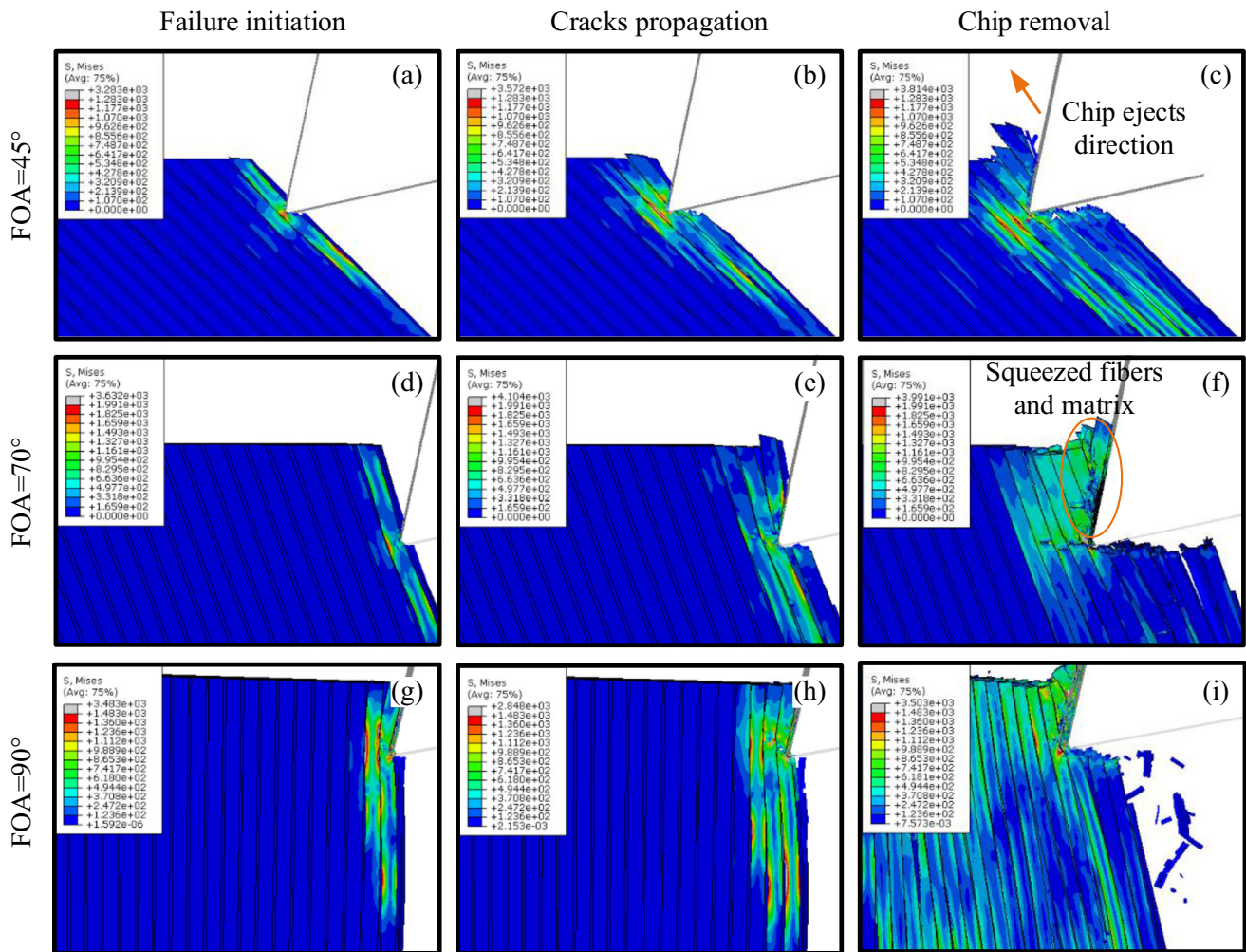


Fig. 7 Cutting mechanism variation of crushing type

however, tends to become easier with less buckling in the fibers. Once the fibers are bended to failure by the rake face, the cracks will stop the propagation along the fiber direction (Fig. 6h and i). The cycle for all the three situations repeats periodically during the whole cutting process.

In the crushing type, the chip formation is characterized by cutting tip crushes of fibers and matrix. Figure 7 shows the typical cutting mechanism of this type. When FOA = 45°, the location of failure initiation is almost exactly in the front of the cutting tip (Fig. 7a). In the contacting area, the fibers and the surrounding matrix are crushed into comminuted fragments due to the combination of shearing and compressing stress. There is not only one crack but actually numerous cracks propagating in the area at the same time. This should be why modeling the chip formation accurately in analytical way is extremely difficult. After being cut by the cutting tip, the fibers are pressed by the rake face and then move upward along fiber orientation (Fig. 7b and c). When FOA = 70°, the failure initiates in a similar way as FOA = 45°, but the chip ejection tends to become more difficult since the shearing trend in fiber direction has reduced (Fig. 7d and e). The broken

fibers and matrix are squeezed by the rake face and the uncut chip. The chip does not form completely until the fibers and matrix are crushed (Fig. 7e and f). For this reason, the energy consumed in cutting of FOA = 70° must be much more than that in cutting of FOA = 45°. When FOA = 90°, the failure initiates causing large bending-induced stress in the sub-surface (Fig. 7g). The bending-induced stress has already been observed since FOA = 10°. The stress transfers deeper and deeper to the sub-surface as FOA increases from 10° to 90° (Figs. 6dd and 7a, d, and g). This explains the variation of sub-surface damage (discussed in section 4.4). The chip formation is getting more difficult than FOA = 70° (Fig. 7h and i) and much more energy will be consumed.

The distinct feature of the bending type is the extensive large deformation of the fibers and the matrix in the cutting area. Figure 8 shows the cutting mechanism of the bending type. When FOA = 135°, the fibers and matrix are bended by the rake face. The failure initiation occurs as the bending-induced stress in fibers exceeds the strength (Fig. 8a). The crack propagation tends to become more complicated than that in the crushing type. This is because the location of failure

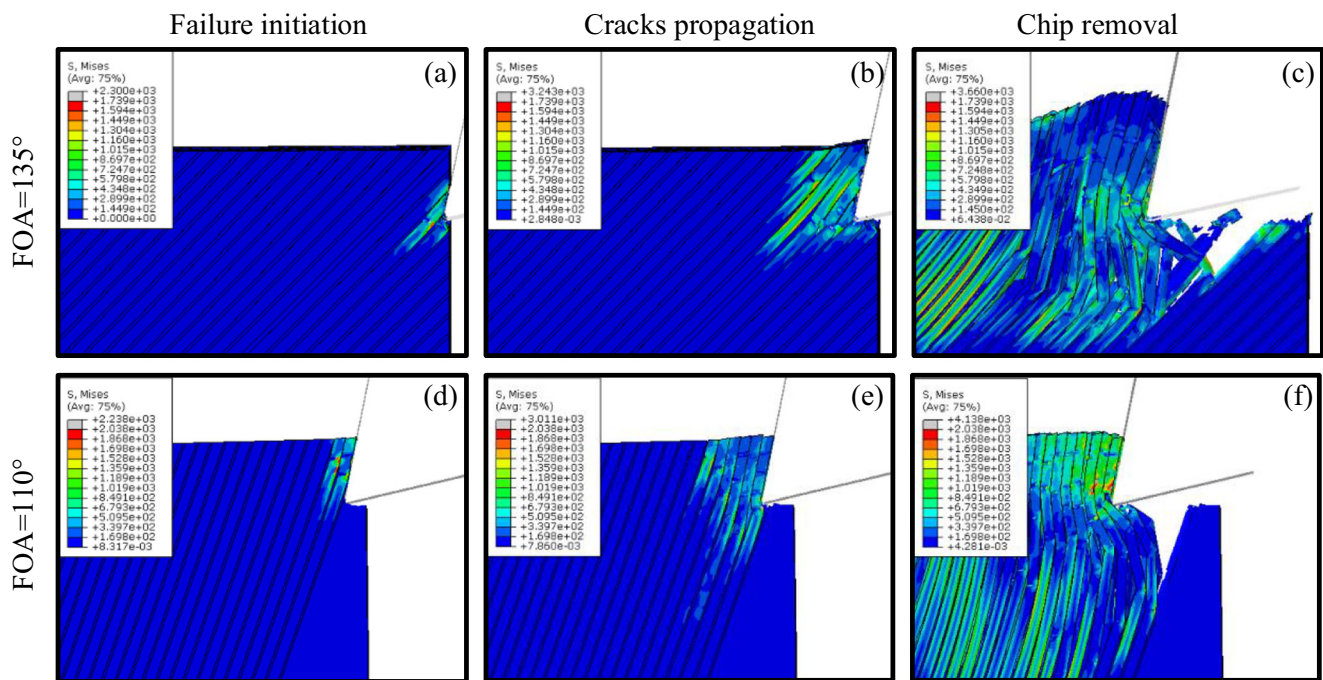


Fig. 8 Cutting mechanism variation of bending type

in the fibers and matrix is not only in the front of the cutting tip but scatters in the whole cutting area (Fig. 8b and c). After being bended by the rake face, the fibers and matrix are finally separated by the shearing of the cutting tip (Fig. 8c). As FOA decreases to 110° , the bending effect decreases and the shearing effect increases (Fig. 8d and e). Consequently, better sub-surface quality is obtained than that in $FOA = 135^\circ$ (Fig. 8f). It should be noted that the bending-induced deformation is always annoying for CFRP cutting. The chips accumulate in front of the rake face because they cannot be ejected easily. The pressure from the rake face is transmitted forward causing more interface debonding and severer sub-surface damage. Therefore, the bending needs to be reduced at any cost to improve cutting quality. On the contrary, the contribution of the cutting tip needed to be enhanced as it offers shearing and concentrate compressive load in the fibers and matrix, which helps to break the fibers in an ideal position.

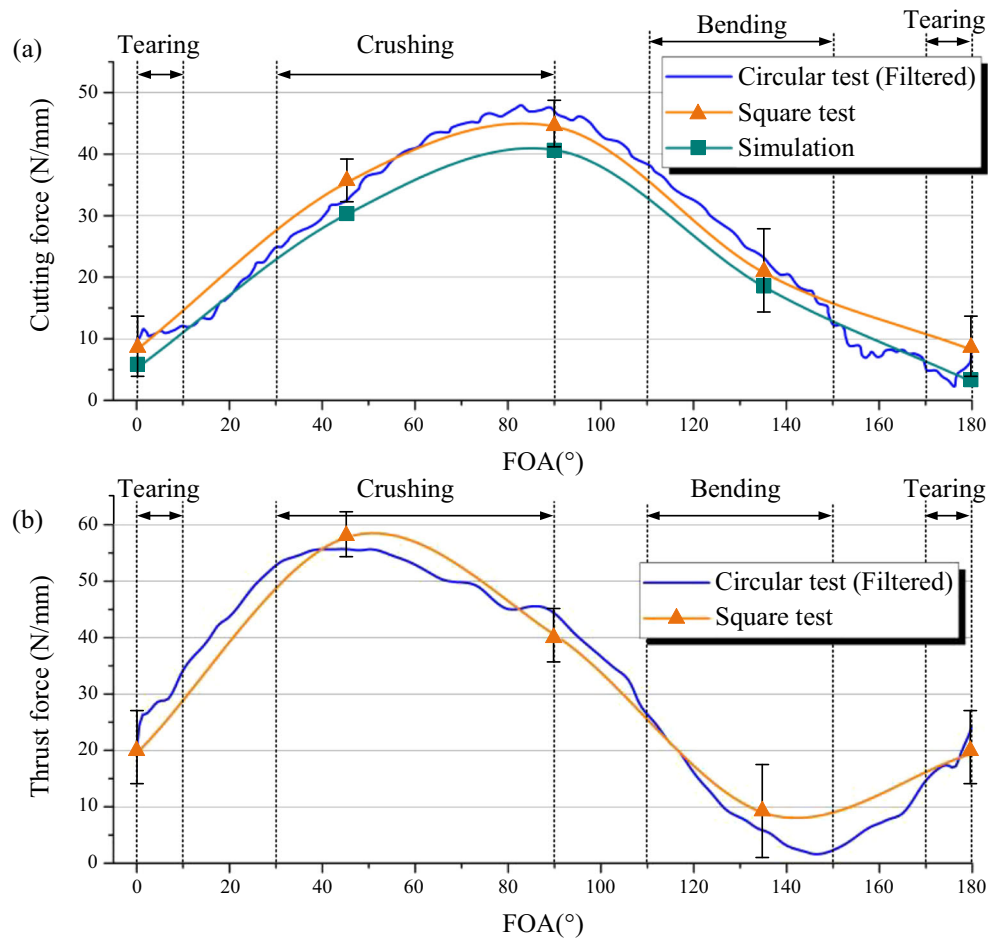
4.3 Variation of the forces in CFRP cutting

As shown in Fig. 9, the forces from the three sources share the same trend. The cutting forces obtained from the circular-cutting test, square-cutting test, and simulation are in good accordance. The thrust forces obtained from circular- and square-cutting tests are also in the same level. The thrust force in simulation, however, was not able to predict since the element delete technique was involved. A similar phenomenon was also reported in literature [2, 32]. The forces in cutting are usually taken as an indicator that reflects whether the cutting process is smooth and steady or not. When the forces vary a

lot and experience dramatic fluctuation, it may mean that the cutting system is experiencing vibration and thus, the machining accuracy will be affected. Unfortunately, CFRP cutting is the case. Figure 9 shows the forces in CFRP cutting obtained from square- and circular-cutting tests and the simulation. As can be seen, when the FOA varies from 0° to 180° , the cutting force F_c increases and reaches the peak value at around $FOA = 90^\circ$, and then decreases to the minimum value at around $FOA = 0^\circ$. The thrust force F_t , however, reaches the peak value at around $FOA = 45^\circ$, and then goes down to the minimum value at around $FOA = 150^\circ$, and after that it increases again. Understanding this trend is helpful when studying the interaction of the machine tool and workpiece during drilling, turning, or milling of CFRP, in which situation, the angle between the cutting speed and fiber varies from 0° to 180° periodically.

A reasonable explanation of the force variation can be given by analyzing the cutting mechanism. As discussed in section 4.2, the cutting mechanism experiences tearing, crushing, and bending type in a cycle. Figure 9 shows the corresponding force segment in each type. The energy spent in the tearing type is the least among the three type as it is mainly consumed on debonding the interface. Both the cutting and thrust force in this situation, as a result, are small. When changing to the crushing type, the energy consumption increases as the fibers in front of the cutting tip needs to be cut to form a chip. Consequently, both the cutting and thrust force will increase. As seen from Fig. 10, one can realize why the cutting force keeps increasing until FOA is around 90° , while the thrust force drops at around $FOA = 45^\circ$. The resistance to the cutting

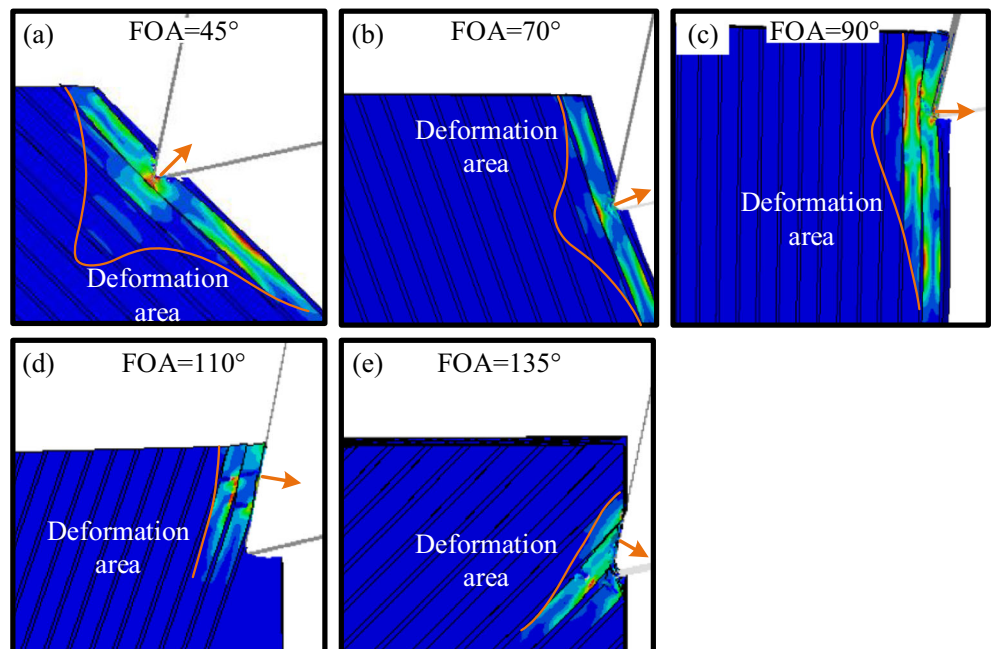
Fig. 9 The variation of **a** cutting force and **b** thrust force



tool can be simply estimated by the deformation area. As FOA increases from 45° to 90°, the deformation trend is getting

close to the cutting direction (Fig. 10a, b, and c), which means the resistance component in the cutting direction (cutting

Fig. 10 Deformation area for different FOAs



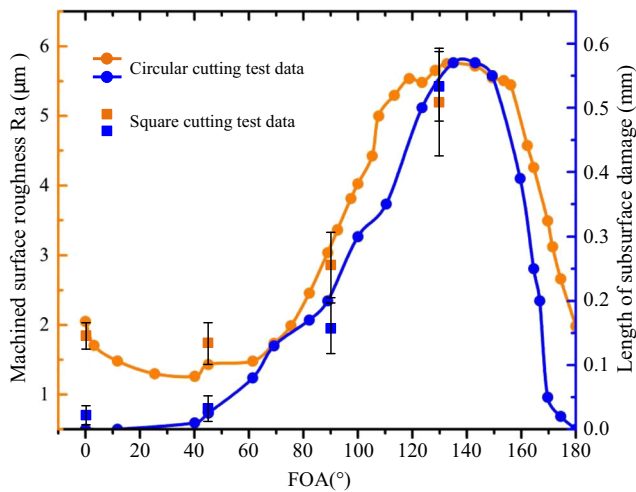


Fig. 11 Machined surface roughness and sub-surface damage distribution on the disk

force) is increasing, while the resistance component in perpendicular to the cutting direction (thrust force) is decreasing. For the bending type, the energy consumption reduces as bending fibers and matrix domain the chip formation. Therefore, the cutting and thrust force will end decreasing again. The thrust force decreases faster than the cutting force as the rake face is pressed downward by the front materials (Fig. 10d and e).

4.4 Machined surface roughness, sub-surface damage, and burr

Machined surface roughness, sub-surface damage, and burr are the three factors that are commonly used to evaluate CFRP machining quality. It is found that there exist correlation in the three factors. Figure 11 shows the machined surface roughness and sub-surface damage obtained by measuring the workpiece in the circular- and square-cutting tests. The data in square test were recorded from four groups of cutting tests. The low machined surface roughness is observed when FOA ranges from 0° to 80°, with the value no higher than

2 µm. Particularly, when FOA is around 45°, the lowest surface roughness is observed. As the FOA goes beyond 90°, the surface roughness increases rapidly. The highest value is observed at around FOA = 135°. The sub-surface damage has almost the same trend. The smallest sub-surface damage is at FOA = 0°, while the largest is at around FOA = 135°. This indicates that better machining quality can be obtained in the tearing and crushing types, while the bending type as a bottleneck constrains the CFRP machining quality.

According to the analysis, it can be concluded that the machined surface roughness has a positive correlation with the sub-surface damage. Figure 12 gives a further explanation of the correlation. In the crushing type (FOA = 45° for example), the fibers tend to break right in front of the cutting tip and little sub-surface damage occurs (Fig. 12a). In the bending type (FOA = 135° for example), however, the fibers tend to break in multiple positions and the damage propagates deeper in the sub-surface (Fig. 12b). When FOA is between 45° and 135°, the value of machined surface roughness and sub-surface damage length may also be an intermediate value. This explains the variation data in Fig. 11.

A phenomenon was found both in the square-cutting test and simulation that the fibers in the margin were unable to be cut but pushed toward the lateral side by the cutting edge, which means the out-of-plane displacement exists extensively in the fibers (Fig. 13a and b). The in-plane displacement assumption, commonly referred when modeling fiber failure in literature, is invalid for CFRP cutting. As the fibers experience extra lateral deformation, the cracks may propagate deeper to the sub-surface in the margin area than in the middle causing severer damage in the margin. After the cutting edge passes, the uncut fibers will bounce back, and thus, the burr forms. The same phenomenon was also found in the circular-cutting test, which is extraordinarily similar to the burr formation in drilling. During drilling, it is quite common that the burr occurs in the exit of the hole. Figure 13c shows a cluster-enlarged burr after drilling by a twist drill. It is more likely that the burr occurs when the major cutting edge encounters the fibers as crushing

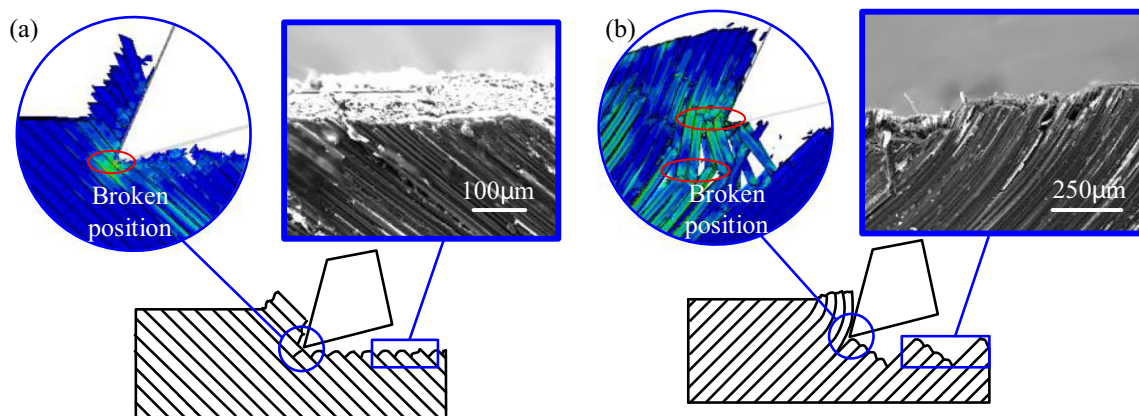


Fig. 12 Machined surface and sub-surface in crushing and bending type

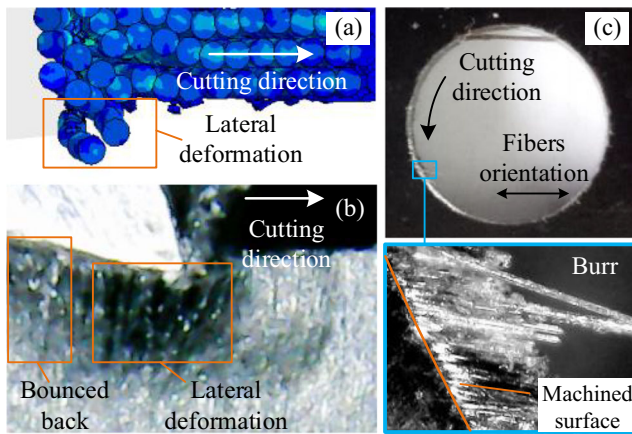


Fig. 13 Burr formation in CFRP cutting: **a** FOA = 90° cutting simulation top view, **b** FOA = 90° square-cutting test side view, and **c** hole exit burr formation in drilling

type, while almost no burr is observed in the bending type area. The burr formation process can be seen in the simulation results, but it cannot be thoroughly explained by the cutting mechanism reported in this study. This limitation exists because the cutting mechanism and its variation is described only in working plane. Further work associating the fiber failure mechanism for out of plane situation needs to be done.

4.5 Effects of rake angle and cutting edge radius

When considering the effects of the rake angle and cutting edge radius, the two most concerned aspects are fiber primary failure and cutting chip removal. Fiber primary failure means

the fiber is broken but has not formed a chip yet. For the rake angle, the general conception is the large rake angle (sharper tool) cutting may get better cutting performance. This conception, however, may not be applicable for all the FOAs. In Ref. [2], the authors found that when FOA = 135°, large rake angle tool can provide concentrated stress in the fibers. Then, the fibers can be cut rather than bended to failure. Thus, the forces in cutting will be reduced and tool life will increase. Though both of the fiber primary failure and cutting chip removal can be achieved easier for large rake angle cutting, it is still unacceptable as it makes tool edge wear and collapse easily. Moreover, cutting CFRP with a large rake angle may not have the desired advantages especially when FOA > 90°. Figure 14 shows the effects of the rake angle on chip formation when cutting FOA = 45° and 135°. For FOA = 45°, when the rake angle is 0°, the chips tend to accumulate in front of the cutting tip and cannot be ejected immediately. The accumulated chips keep compressing the uncut chip causing extra deformation in the area (Fig. 14a). When the rake angles are 4° and 12°, however, there are very little chips accumulated in front of the cutting tip and the chip removal process is getting more fluent (Fig. 14b and c). For FOA = 135°, the rake angle has a more significant influence. When the rake angle is 4° (Fig. 14d), the advantage is the fibers are bended harder so that fibers break easier. The shearing stress in front of the cutting tip is more concentrated and thus, the fibers' failure positions will locate nearer to the cutting tip. The disadvantage is the chip's removal becomes very difficult. The fibers in front of the rake face are pushed forward instead of upward. Then, the fibers have no choice but move toward the lateral

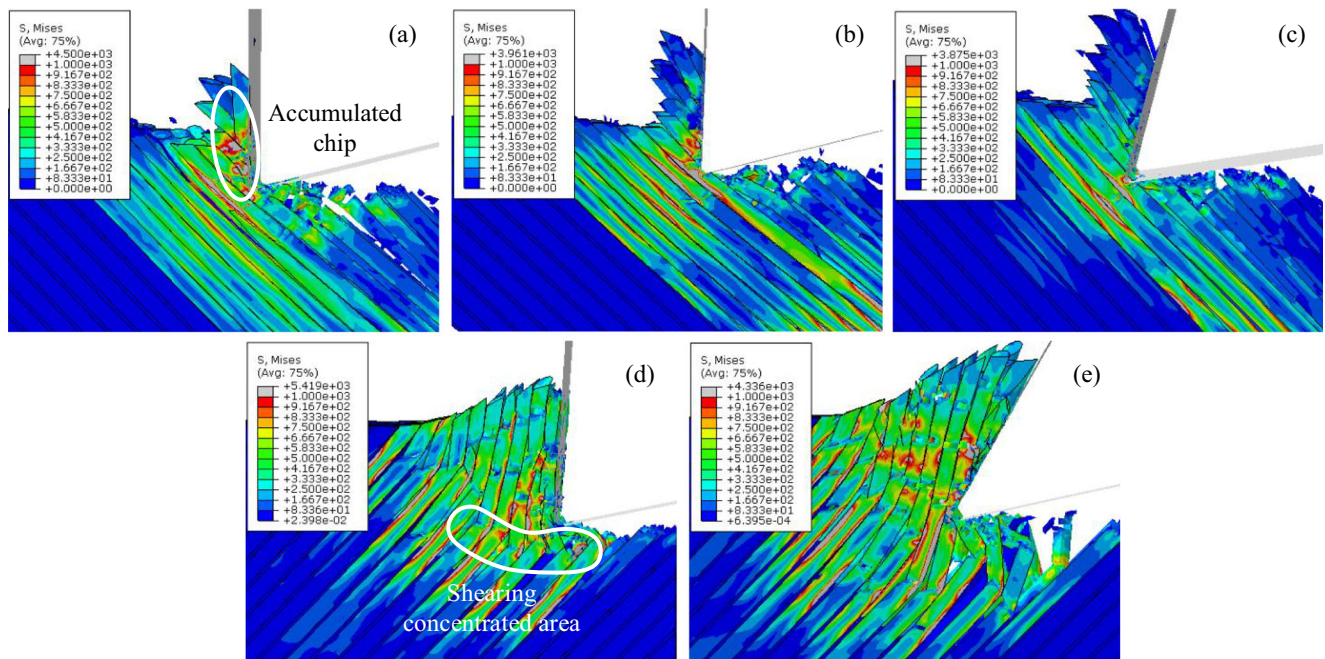


Fig. 14 Effects of rake angle: **a** FOA = 45°, rake angle is 0°; **b** FOA = 45°, rake angle is 4°; **c** FOA = 45°, rake angle is 12°; **d** FOA = 135°, rake angle is 4°; **e** FOA = 135°, rake angle is 30°; **f** FOA = 135°, double rake angle (4° and 30°)

side to avoid the cutting wedge. This will cause severer sub-surface damage. When the rake angle is 30° (Fig. 14e), the chip removal may get easier than a 4° rake angle but the shearing stress offered by the cutting tip becomes less concentrated. Then, the fibers tend to break in multiple positions which will decrease the machined surface roughness. Based on the discussion in section 4.2 and this section, it can be concluded that the optimization of cutting tool geometry for FOA $> 90^\circ$ is primarily about making the chip removal easier with the least effects on the uncut area.

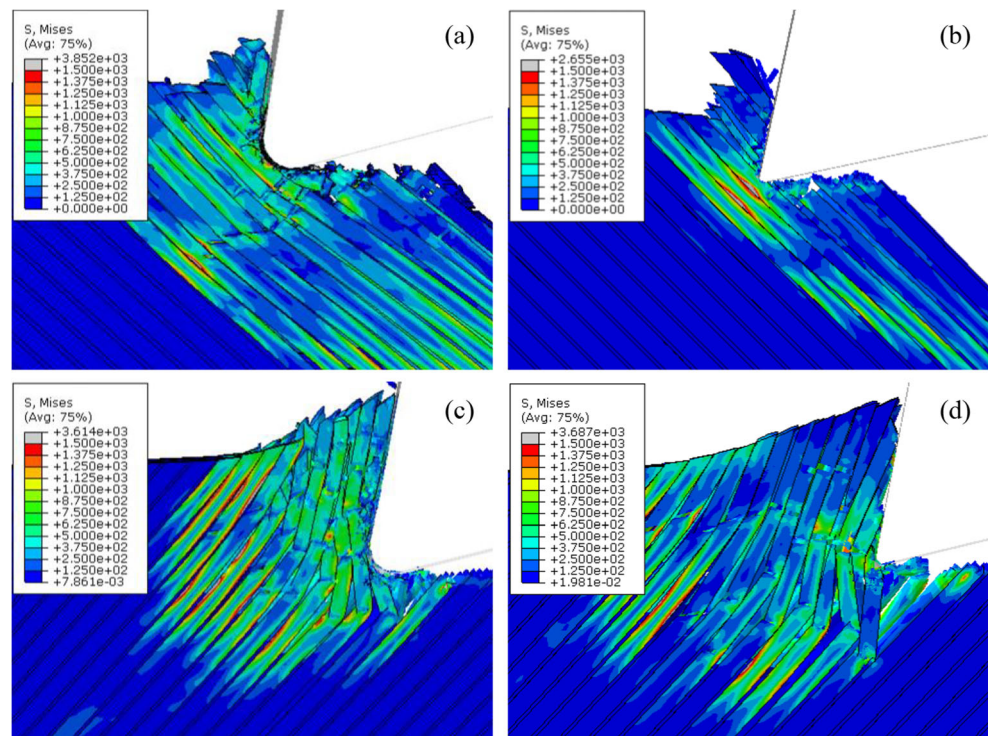
The cutting edge radius has more effects on fiber's primary failure than chip removal. Figure 15 shows the effects of the cutting edge radius on chip formation when FOA = 45° and 135° . The cutting edge radius in Fig. 15a and c is four times larger than that in Fig. 15b and d). For FOA = 45° , when cutting with a large edge radius, the fibers need to be pushed further distance before being cut, which will cause larger deformation in sub-surface. Meanwhile, the machined surface tends to be worse compare with cutting with small edge radius. For FOA = 135° , however, the chip formation is less sensitive to the cutting edge radius. This is because the fiber's primary failure is mainly controlled by the rake face. The radius of the cutting edge has no significant effects on the shearing stress distribution in front of the cutting tip. The chip removal will always be difficult in this situation regardless of the radius of cutting edge.

5 Conclusions and outlook

Based on the numerical and experimental results, the following conclusions are obtained:

1. CFRP cutting mechanism varies gradually when FOA increases from 0° to 180° . The cutting mechanism is summarized into three types, namely tearing type, crushing type, and bending type. It was found that the forces, machined surface roughness, sub-surface damage, and burr are highly dependent on the cutting mechanism. Of the three types, the chip removal is the most difficult in bending type.
2. Cutting force and thrust force vary regularly and continuously according to the cutting mechanism. The largest and smallest cutting forces are obtained at around FOA = 90° and 0° , respectively, while the largest and smallest thrust force are obtained at around FOA = 45° and 150° respectively.
3. The machined surface roughness and the sub-surface damage were found to have a positive relation. When $0^\circ < \text{FOA} < 80^\circ$, lower machined surface roughness and less sub-surface damage length are obtained, with the value no higher than $2 \mu\text{m}$ (Ra) and 0.15 mm respectively. Both their worst values are obtained at around FOA = 135° . The results of the two aspects indicate that the bottleneck of CFRP machining occurs when FOA is around 135° .

Fig. 15 Effect of cutting edge radius: **a** FOA = 45° , tool radius equals two times of fiber radius; **b** FOA = 45° , tool radius equals half time of fiber radius; **c** FOA = 135° , tool radius equals two times of fiber radius; **d** FOA = 135° , tool radius equal half time of fiber radius



4. The burr generates due to the extensive out of plane deformation in the margin fibers. The fibers in the very outside are not cut but pushed towards to lateral side by the cutting edge. Then the fibers bounce back to form burrs.
5. The rake angle plays a key role in chip removal especially when FOA > 90°. For a large rake angle, though the chip slides on the rake face easily, the cutting edge also gets collapsed easily. A new tool geometry with two rake angles will help to improve the machinability of CFRP. The cutting edge radius was found to have significant effects on fiber's primary failure but has no significant effects on chip removal.

In actual cutting situation, though cracks occur in the matrix, parts of them will still remain in the intervals of the fibers and keep constraining the fibers. In this simulation, however, once the matrix elements are deleted, the fibers are totally free and will move further before being cut than in the real situation. Therefore, more work should be done to compensate for the drawbacks. Moreover, the cutting mechanism should not only be studied in working plane. The out of plane deformation of fibers should also be involved. Three-dimensional cutting mechanism needs to be investigated.

Acknowledgments This work is supported by the Natural Science Foundation Guiding Program of Liaoning province [Grant numbers 2019-ZD-0235] and the Doctoral Foundation of SAU [Grant numbers 19YB13].

References

1. Cheng H, Gao J, Kafka OL, Zhang K, Luo B, Liu WK (2017) A micro-scale cutting model for UD CFRP composites with thermo-mechanical coupling. *Compos Sci Technol* 153:18–31
2. Calzada KA, Kapoor SG, Devor RE, Samuel J, Srivastava AK (2012) Modeling and interpretation of fiber orientation-based failure mechanisms in machining of carbon fiber-reinforced polymer composites. *J Manuf Process* 14(2):141–149
3. Gao C, Xiao J, Xu J, Ke Y (2016) Factor analysis of machining parameters of fiber-reinforced polymer composites based on finite element simulation with experimental investigation. *Int J Adv Manuf Technol* 83(5–8):1113–1125
4. Yan X, Reiner J, Bacca M, Altintas Y, Vaziri R (2019) A study of energy dissipating mechanisms in orthogonal cutting of UD-CFRP composites. *Compos Struct* 220:460–472
5. Liu H, Xie W, Sun Y, Zhang J, Chen N (2018) Investigations on micro-cutting mechanism and surface quality of carbon fiber-reinforced plastic composites. *Int J Adv Manuf Technol* 94(9–12):3655–3664
6. Abena A, Essa K (2019) 3D micro-mechanical modelling of orthogonal cutting of UD-CFRP using smoothed particle hydrodynamics and finite element methods. *Compos Struct* 218:174–192
7. Madhavan V, Lipczynski G, Lane B, Whinton E (2015) Fiber orientation angle effects in machining of unidirectional CFRP laminated composites. *J Manuf Process* 20(S12):431–442
8. Wang DH, Ramulu M, Arola D (1995) Orthogonal cutting mechanisms of graphite/epoxy composite .1. Unidirectional laminate. *Int J Mach Tool Manu* 35(12):1623–1638
9. Wang DH, Ramulu M, Arola D (1995) Orthogonal cutting mechanisms of graphite/epoxy composite .2. Multidirectional laminate. *Int J Mach Tool Manu* 35(12):1639–1648
10. Zitoune R, Collombet F, Lachaud F, Piquet R, Pasquet P (2005) Experiment-calculation comparison of the cutting conditions representative of the long fiber composite drilling phase. *Compos Sci Technol* 65(3–4):455–466
11. Wang XM, Zhang LC (2003) An experimental investigation into the orthogonal cutting of unidirectional fibre reinforced plastics. *Int J Mach Tool Manu* 43(10):1015–1022
12. Henerichs M, Voß R, Kuster F, Wegener K (2015) Machining of carbon fiber reinforced plastics: influence of tool geometry and fiber orientation on the machining forces. *CIRP J Manuf Sci Technol* 9:136–145
13. Wang F, Zhang B, Zhao M, Cheng D, Wang Z (2019) Evolution laws of fiber-matrix interface cracks in machining of carbon fiber reinforced polymer. *Int J Adv Manuf Technol* 101(1–4):963–977
14. Su Y, Jia Z, Niu B, Bi G (2017) Size effect of depth of cut on chip formation mechanism in machining of CFRP. *Compos Struct* 164:316–327
15. Voss R, Seeholzer L, Kuster F, Wegener K (2017) Influence of fibre orientation, tool geometry and process parameters on surface quality in milling of CFRP. *CIRP J Manuf Sci Technol* 18:75–91
16. Voss R, Seeholzer L, Kuster F, Wegener K (2019) Analytical force model for orthogonal machining of unidirectional carbon fibre reinforced polymers (CFRP) as a function of the fibre orientation. *J Mater Process Technol* 263:440–469
17. Li H, Qin X, He G, Jin Y, Sun D, Price M (2016) Investigation of chip formation and fracture toughness in orthogonal cutting of UD-CFRP. *Int J Adv Manuf Technol* 82(5–8):1079–1088
18. Niu B, Su Y, Yang R, Jia Z (2016) Micro-macro-mechanical model and material removal mechanism of machining carbon fiber reinforced polymer. *Int J Mach Tools Manuf* 111:43–54
19. Qi Z, Zhang K, Cheng H, Wang D, Meng Q (2015) Microscopic mechanism based force prediction in orthogonal cutting of unidirectional CFRP. *Int J Adv Manuf Technol* 79(5–8):1209–1219
20. Zenia S, Ben Ayed L, Nouari M, Delameziere A (2015) Numerical analysis of the interaction between the cutting forces, induced cutting damage, and machining parameters of CFRP composites. *Int J Adv Manuf Technol* 78(1–4):465–480
21. Usui S, Wadell J, Marusich T (2014) Finite element modeling of carbon fiber composite orthogonal cutting and drilling. In: Dornfeld D, Helu M (eds) *Procedia CIRP* 211–216
22. Rao GVG, Mahajan P, Bhatnagar N (2008) Three-dimensional macro-mechanical finite element model for machining of unidirectional-fiber reinforced polymer composites. *Mater Sci Eng A Struct* 498(1–2SI):142–149
23. Nayak D, Bhatnagar N, Mahajan P (2005) Machining studies of ud-frp composites part 2: finite element analysis. *Mach Sci Technol* 9(4):503–528
24. Iliescu D, Gehin D, Iordanoff I, Girot F, Gutierrez ME (2010) A discrete element method for the simulation of CFRP cutting. *Compos Sci Technol* 70(1):73–80
25. Rao GVG, Mahajan P, Bhatnagar N (2007) Machining of UD-GFRP composites chip formation mechanism. *Compos Sci Technol* 67(11–12):2271–2281
26. Kawabata S (1990) Measurement of the transverse mechanical-properties of high-performance fibers. *J Text I* 81(4):432–447

27. Hobbiebrunken T, Fiedler B, Hop M, Ochial S, Schulte K (2005) Microscopic yielding of CF/epoxy composites and the effect on the formation of thermal residual stresses. *Compos Sci Technol* 65(10): 1626–1635
28. Jordan JL, Foley JR, Siviour CR (2008) Mechanical properties of Epon 826/DEA epoxy. *Mech Time Depend Mater* 12(3):249–272
29. Kaddour AS, Hinton MJ, Smith PA, Li S (2013) Mechanical properties and details of composite laminates for the test cases used in the third world-wide failure exercise. *J Compos Mater* 47(20-21SI): 2427–2442
30. Zhang B, Wu Y, Yang Z, Wang X (2011) Experimental investigation of the longitudinal compressive strength of carbon fibres with a direct measurement system. *Polym Polym Compos* 19(6):477–483
31. Isbilir O, Ghassemieh E (2012) Finite element analysis of drilling of carbon fibre reinforced composites. *Appl Compos Mater* 19(3–4): 637–656
32. Abena A, Soo SL, Essa K (2017) Modelling the orthogonal cutting of UD-CFRP composites: development of a novel cohesive zone model. *Compos Struct* 168:65–83

Publisher's note Springer Nature remains neutral with regard to jurisdictional claims in published maps and institutional affiliations.